PROCEEDINGS OF SCIENCE

Measurements of $W\gamma$ and $Z\gamma$ production in pp collisions at $\sqrt{s} = 7$ TeV with the ATLAS detector at the LHC

Zhijun Liang*, **On behalf of the ATLAS collaboration**
University of Oxford
E-mail: zhijun.liang@cern.ch

The integrated and differential fiducial cross sections for the production of a W or Z boson in association with a high-energy photon are measured using pp collisions at $\sqrt{s}$ = 7 TeV. The analyses use a data sample with an integrated luminosity of 4.6 fb^{-1} collected by the ATLAS detector during the 2011 LHC data-taking period. Events are selected using leptonic decays of the W and Z bosons ($W(e\nu, \mu\nu)$ and $Z(e^+e^-, \mu^+\mu^-, \nu\bar{\nu})$) with the requirement of an associated isolated photon. The data are used to test the electroweak sector of the Standard Model and search for evidence for new phenomena. The measurements are used to probe the anomalous $WW\gamma$, $ZZ\gamma$ and $Z\gamma\gamma$ triple-gauge-boson couplings and to search for the production of vector resonances decaying to $Z\gamma$ and $W\gamma$. No deviations from Standard Model predictions are observed and limits are placed on anomalous triple-gauge-boson couplings and on the production of new vector meson resonances.

XXI International Workshop on Deep-Inelastic Scattering and Related Subject -DIS2013,
22-26 April 2013
Marseilles,France

*Speaker.

PoS(DIS 2013)098

1. Introduction

The Standard Model (SM) has proved to provide an accurate description of the production of elementary particles observed in high energy physics experiments. The high-energy proton–proton collisions provided by the LHC explore the production of $W\gamma$ and $Z\gamma$ pairs in a new energy domain. The high center-of-mass energy also allows searches for new particles, for example techni-mesons which are predicted in Technicolor models [1, 2], that decay to these final states.

The measurements of $W\gamma$ and $Z\gamma$ final states from $p\bar{p}$ and pp production have been made at the LHC by the ATLAS [3] collaborations. The measurements presented here are improvements on previous studies of the hadroproduction of $W\gamma$ and $Z\gamma$ pairs, as more precise measurements are performed with a larger data sample. The selected events correspond to 4.6 fb^{-1} of pp collisions recorded by the ATLAS detector in 2011 at a center-of-mass energy of 7 TeV. The diboson candidate events are selected from the production processes $pp \to \ell\nu\gamma + X$ ($\ell = e, \mu$), $pp \to \ell^+\ell^-\gamma + X$ and $pp \to \nu\bar{\nu}\gamma + X$.

2. $W\gamma$ and $Z\gamma$ event selection

The inclusive $W\gamma$ cross-section measurements uses $\ell\nu\gamma$ events, selected by requiring exactly one lepton with $p_{\mathrm{T}} > 25$ GeV, at least one isolated photon with $E_{\mathrm{T}}^{\gamma} > 15$ GeV and $E_{\mathrm{T}}^{\mathrm{miss}}$ above 35 GeV, where $E_{\mathrm{T}}^{\mathrm{miss}}$ is the missing transverse energy measured in the ATLAS calorimeter systems. In addition, the transverse mass[1] of the lepton–$E_{\mathrm{T}}^{\mathrm{miss}}$ system (m_{T}) is required to be greater than 40 GeV. A Z-veto requirement is applied in the electron channel of the $W\gamma$ analysis by requiring that the electron–photon invariant mass ($m_{e\gamma}$) is not within 15 GeV of the Z boson mass (m_Z), where m_Z value is taken from particle data group [4]. This is to suppress the background where one of the electrons from the Z boson decay is mis-identified as a photon.

The inclusive $Z\gamma$ cross-section measurements uses $\ell^+\ell^-\gamma$ events, selected by requiring exactly two oppositely charged same-flavor leptons with an invariant mass greater than 40 GeV, and one isolated photon with $E_{\mathrm{T}}^{\gamma} > 15$ GeV.

The inclusive $Z\gamma$ cross-section measurements also uses $\nu\bar{\nu}\gamma$ events, selected by requiring one isolated photon with $E_{\mathrm{T}}^{\gamma} > 100$ GeV and $E_{\mathrm{T}}^{\mathrm{miss}} > 90$ GeV. The reconstructed photon, $E_{\mathrm{T}}^{\mathrm{miss}}$ and jets (if jets are found) are required to be well separated in the transverse plane with $\Delta\phi(E_{\mathrm{T}}^{\mathrm{miss}}, \gamma) > 2.6$ and $\Delta\phi(E_{\mathrm{T}}^{\mathrm{miss}}, \text{jet}) > 0.4$, in order to reduce the γ+jet background. Events with identified electrons and muons are vetoed to reject W+jets and $W\gamma$ background. The selection criteria to identify the electrons and muons are the same as in the $Z(\ell^+\ell^-)\gamma$ analysis.

In both the $\ell\nu\gamma$ and $\ell^+\ell^-\gamma$ analyses, a selection requirement $\Delta R(\ell, \gamma) > 0.7$ is applied to suppress the contributions from FSR photons in the W and Z boson decays. The events with no jets with $E_{\mathrm{T}} > 30$ GeV are used to measure the exclusive $V\gamma$ ($V = W$ or Z) cross sections.

3. Background Estimation

In the measurements of $\ell\nu\gamma$, $\ell^+\ell^-\gamma$ and $\nu\bar{\nu}\gamma$ production, the background contributions are es-

[1] $m_{\mathrm{T}} = \sqrt{2p_{\mathrm{T}}(\ell) \times E_{\mathrm{T}}^{\mathrm{miss}} \times (1 - \cos\Delta\phi)}$, and $\Delta\phi$ is the azimuthal separation between the directions of the lepton and the missing transverse momentum vector.

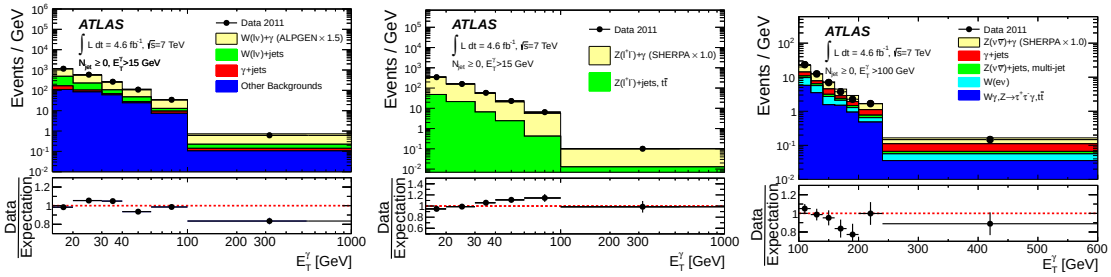

(a) (b) (c)

Figure 1: Photon transverse energy from the selected (a) $l\nu\gamma$ events, (b) $\ell^+\ell^-\gamma$ events, (c) $\nu\bar{\nu}\gamma$ events [3].

timated either from simulation or from data. The backgrounds estimated from data include W+jets and γ+jets for the $\ell\nu\gamma$ final state. It is found that the contribution from W+jets process is about 15% and the contribution from γ+jets is about 10% in selected $\ell\nu\gamma$ candidates. Based on data-driven estimation, Z+jets contribution to the $\ell^+\ell^-\gamma$ final state is found to be about 15%. Z+jets, multi-jets, γ+jets and events with an electron faking a photon for the $\nu\bar{\nu}\gamma$ final state are also estimated from data, their contributions to $\nu\bar{\nu}\gamma$ candidates are about 45% in total.

Additional backgrounds from other processes, such as $Z(\ell^+\ell^-)+X$, $t\bar{t}$, WW, single top quark, $Z(\tau^+\tau^-)$ and $W(\tau\nu)$ for the $W\gamma$ analysis, $t\bar{t}$ and $l\nu\gamma$ for $Z\gamma$ analysis, are estimated from simulation.

The distributions of the photon transverse energy from the selected $W\gamma$ and $Z\gamma$ events are shown in Fig. 1. The data are compared to the sum of the backgrounds and the SM signal predictions. The distributions for the expected $V\gamma$ signal are taken from signal MC simulation and normalized to the total extracted number of signal events.

4. Cross-Section Measurements

The cross-section measurements for the $W\gamma$ and $Z\gamma$ processes are performed in the fiducial region, defined at particle level using the object and event kinematic selection criteria described in Sec. 2. The cross-section measurements for the processes $pp \to \ell\nu\gamma+X$ and $pp \to (\ell^+\ell^-\gamma/\nu\bar{\nu}\gamma)+X$ are calculated as

$$\sigma^{\text{ext}-\text{fid}}_{pp\to\ell\nu\gamma(\ell^+\ell^-\gamma/\nu\bar{\nu}\gamma)} = \frac{N^{\text{sig}}_{V\gamma}}{A_{V\gamma}\cdot C_{V\gamma}\cdot\int \mathscr{L}dt.} \tag{4.1}$$

where $N^{\text{sig}}_{W\gamma}$ and $N^{\text{sig}}_{Z\gamma}$ denote the number of $W\gamma$ and $Z\gamma$ signal events, $\int \mathscr{L}dt$ denotes the integrated luminosity for the analysis. $C_{V\gamma}$ is defined as the number of reconstructed MC events passing all selection requirements divided by the number of generated events at particle level within the fiducial region. The dominant uncertainties on $C_{V\gamma}$ come from photon identification and isolation efficiency (5%). $A_{V\gamma}$ are the acceptances, defined at particle level as the number of generated events found within the fiducial region divided by the number of generated events within the extended fiducial region. The systematic uncertainties for $A_{W\gamma}$ and $A_{Z\gamma}$ are dominated by parton distribution functions uncertainties (<0.8%), by the renormalization and factorization scale uncertainties (<0.5%) and by the uncertainties on the size of the contributions from fragmentation photons (<0.3%).

	$\sigma^{\text{ext}-\text{fid}}$[pb] Measurement	$\sigma^{\text{ext}-\text{fid}}$[pb] MCFM Prediction
	$N_{\text{jet}} \geq 0$	
$\ell\nu\gamma$	2.77 ± 0.03 (stat) ± 0.33 (syst) ± 0.14 (lumi)	1.96 ± 0.17
$\ell^+\ell^-\gamma$	1.31 ± 0.02 (stat) ± 0.11 (syst) ± 0.05 (lumi)	1.18 ± 0.05
$\nu\bar{\nu}\gamma$	0.133 ± 0.013 (stat) ± 0.020 (syst) ± 0.005 (lumi)	0.156 ± 0.012
	$N_{\text{jet}} = 0$	
$\ell\nu\gamma$	1.76 ± 0.03 (stat) ± 0.21 (syst) ± 0.08 (lumi)	1.39 ± 0.13
$\ell^+\ell^-\gamma$	1.05 ± 0.02 (stat) ± 0.10 (syst) ± 0.04 (lumi)	1.06 ± 0.05
$\nu\bar{\nu}\gamma$	0.116 ± 0.010 (stat) ± 0.013 (syst) ± 0.004 (lumi)	0.115 ± 0.009

Table 1: Measured cross sections for the $\ell\nu\gamma$, $\ell^+\ell^-\gamma$ and $\nu\bar{\nu}\gamma$ processes at $\sqrt{s} = 7$ TeV in the fiducial region [3].

The measured production cross sections in the fiducial region for the $\ell\nu\gamma$, $\ell^+\ell^-\gamma$ and $\nu\bar{\nu}\gamma$ processes are summarized in Table 1. These cross section measurements are the most extensive made to date for the study of V+γ production at the LHC.

Fig. 2 shows the differential fiducial cross sections as a function of E_{T}^{γ} in $V\gamma$ processes with the inclusive selection and with the exclusive zero-jet selection, as well as a comparison to the SM prediction.

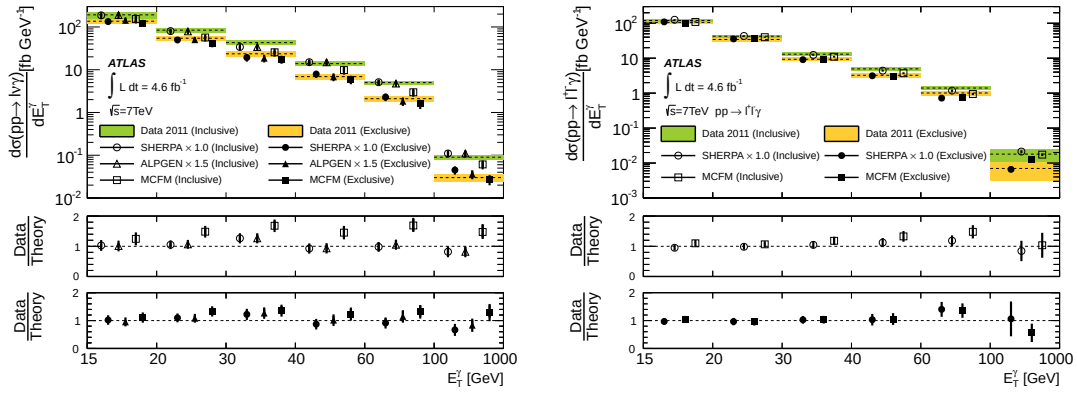

(a) (b)

Figure 2: Measured E_{T}^{γ} differential cross sections of (a) the $pp \to \ell\nu\gamma$ process and of (b) the $pp \to \ell^+\ell^-\gamma$ process, using combined electron and muon measurements in the inclusive ($N_{\text{jet}} \geq 0$) and exclusive ($N_{\text{jet}} = 0$) extended fiducial regions [3]. The lower plots show the ratio of the data to the predictions by different generators.

5. Limits on Anomalous Triple-Gauge-Boson Couplings

The reconstructed E_{T}^{γ} distributions from $V\gamma$ events with the exclusive zero-jet selection are used to set limits on $WW\gamma$, $ZZ\gamma$ and $Z\gamma\gamma$ anomalous triple-gauge-boson coupling parameters. Assuming C and P conservation separately, the aTGCs are generally chosen as λ_{γ}, $\Delta\kappa_{\gamma}$ ($\Delta\kappa_{\gamma} = \kappa_{\gamma} - 1$)

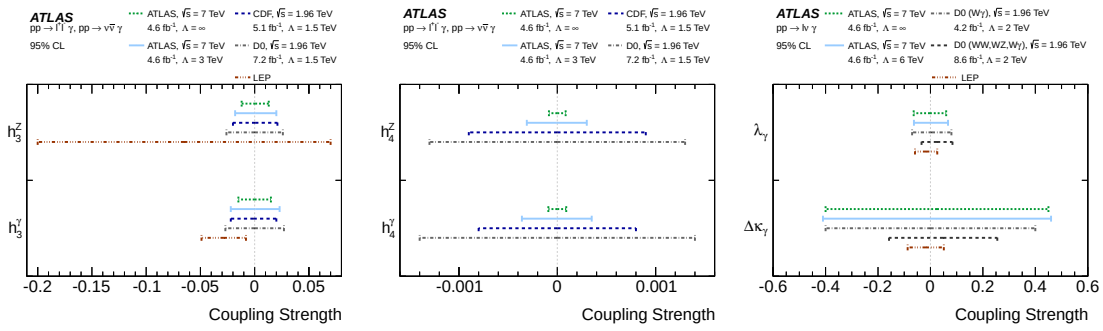

Figure 3: The 95% CL intervals for anomalous couplings from ATLAS [3], D0 [11, 12], CDF [10] and LEP [9] for (a),(b) the neutral aTGCs h_3^γ, h_3^Z, h_4^γ, h_4^Z as obtained from $Z\gamma$ events, and (c) the charged aTGCs $\Delta\kappa_\gamma$, λ_γ. The integrated luminosities and new-physics scale parameter Λ are shown. The ATLAS and D0 results for the charged aTGCs measured from $W\gamma$ production are shown. Except for the coupling under study, all other anomalous couplings are set to zero.

for the $WW\gamma$ vertex [6, 7], h_3^Z, h_4^Z for the $ZZ\gamma$ vertex [8], and h_3^γ, h_4^γ for the $Z\gamma\gamma$ vertex [8]. Form factors are introduced to avoid unitarity violation at very high energy. Typical choices of these form factors for the $WW\gamma$ aTGCs are: $\Delta\kappa_\gamma(s) = \Delta\kappa_\gamma/(1+\hat{s}/\Lambda^2)^2$ and $\lambda_\gamma(s) = \lambda_\gamma/(1+\hat{s}/\Lambda^2)^2$ [7]. For the $ZZ\gamma$ aTGCs, conventional choices of form factors are $h_3^Z(s) = h_3^Z/(1+\hat{s}/\Lambda^2)^3$ and $h_4^Z(s) = h_4^Z/(1+\hat{s}/\Lambda^2)^4$ [8]. Similar choices of form factors are used for $Z\gamma\gamma$ aTGCs. Here $\sqrt{\hat{s}}$ is the $W\gamma$ or $Z\gamma$ invariant mass and Λ is the new-physics energy scale. To conserve unitarity, Λ is chosen as 6 TeV in the $W\gamma$ analysis and 3 TeV in the $Z\gamma$ analysis. The results with energy cut-off $\Lambda = \infty$ are also presented as a comparison in the unitarity violation scheme.

The limits are defined as the values of aTGCs that demarcate the central 95% of the integral of the likelihood distribution. The resulting allowed ranges for the anomalous couplings are shown in Fig. 3 for $WW\gamma$, $ZZ\gamma$ and $Z\gamma\gamma$, are also compared with the results from LEP [9] and the Tevatron [10, 11, 12].

6. Search for narrow resonances

Models such as Technicolor (TC) predict spin-1 mesons that have significant branching ratios to $W\gamma$ and $Z\gamma$. The discovery of a particle compatible with the SM Higgs [13, 14] does not exclude the full phase space of the TC models [15, 16, 17]. Therefore, they are used here as a benchmark for new physics processes that would appear as new resonant $W\gamma$ and $Z\gamma$ states. The Technicolor Strawman [18] model implemented in PYTHIA [19] is used to describe the production and decay of neutral and charged techni-mesons: $\omega_T \to Z\gamma$ and $a_T \to W\gamma$.

For the $\omega_T \to Z\gamma$ channel, the $m^{Z\gamma}$ distribution is fit by the sum of a Crystal-Ball function (CB) [20, 21, 22]. For the $a_T \to W\gamma$ channel, the $m_T^{W\gamma}$ distribution is fit by a CB function. The double-exponential function is found to reproduce the shapes of all these distributions properly, and is therefore used for the SM background estimation.

The parameter of interest used in this analysis is the fiducial cross section of an eventual new physics signal. σ_{Fid} is scanned to check the compatibility of the data with a background only or a signal plus background hypothesis.

The statistical test used is based on the Profile Likelihood Ratio [23] $L(\sigma_{\text{Fid}})$, to test different hypothesized values of σ_{Fid}. $L(\sigma_{\text{Fid}})$ is built from the likelihood function describing the probability density function of $m^{Z\gamma}$ and $m_T^{W\gamma}$ under a signal plus background hypothesis and the systematic uncertainties. It combines both electron and muon final states. The statistical tests are then performed on the $m_T^{W\gamma}$ and $m^{Z\gamma}$ distributions.

Figure 4 (b) shows the expected and observed limits obtained for $a_{\text{T}} \to W\gamma$. The largest deviation is observed at $m_{a_{\text{T}}} = 285$ GeV where an upward fluctuation is recorded with a p-value of $p_0 \approx 0.05$ or a local significance of 2.0σ. In the $W\gamma$ channel the expected mass limit on the Low Scale Technicolor (LSTC) production of a_{T} is $m_{a_{\text{T}}} = 619$ GeV, while the observed limit is $m_{a_{\text{T}}} = 703$ GeV.

These results are similar to those from previous searches for LSTC [24, 25] in other channels. They are more stringent than previous limits from vector resonance searches at Tevatron [26] in the $Z\gamma$ final state and they are the first limits to be set from single resonance searches in the $W\gamma$ channel.

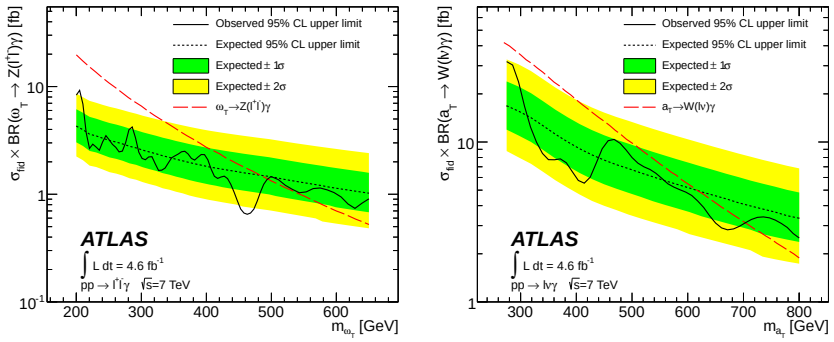

(a) (b)

Figure 4: 95% CL limits on narrow vector resonance production obtained using $\mathscr{L} = 4.6$ fb^{-1} of data for (a) the $pp \to \ell^+\ell^-\gamma$ final state and for (b) the $pp \to \ell\nu\gamma$ final state [3]. The parameterization of LSTC [27, 28] used to benchmark the observed limit is obtained using $m_{\rho_{\text{T}}} = m_W - m_{\pi_{\text{T}}}$.

References

[1] S. Weinberg, Phys. Rev. D **19**, 1277 (1979).

[2] L. Susskind, Phys. Rev. D **20**, 2619 (1979).

[3] ATLAS Collaboration, Phys. Rev. D **87**, 112003 (2013).

[4] J. Beringer *et al.*, Particle Data Group, Phys. Rev. D **86**, 010001 (2012).

[5] ATLAS Collaboration, JINST **3**, S08003 (2008).

[6] U. Baur and E. L. Berger, Phys. Rev. D **41**, 1476 (1990).

[7] U. Baur, T. Han, and J. Ohnemus, Phys. Rev. D **48**, 5140 (1993).

[8] U. Baur and E. L. Berger, Phys. Rev. D **47**, 4889 (1993).

[9] The LEP Collaborations: ALEPH, DELPHI, L3, OPAL, and the LEP Electroweak Working Group. arXiv:0612034.

[10] F. Abe *et al.*, CDF Collaboration, Phys. Rev. D **107**, 051802 (2011).

[11] V. Abazov *et al.*, D0 Collaboration, Phys. Rev. Lett. **100**, 241805 (2008) .

[12] V. Abazov *et al.*, D0 Collaboration, Phys. Rev. D **85**, 052001 (2012).

[13] ATLAS Collaboration, Phys. Lett. B **716**, 1 (2012).

[14] CMS Collaboration, Phys. Lett. B **716**, 30 (2012).

[15] E. Eichten, K. Lane, and A. Martin, arXiv:hep-ph/1210.5462.

[16] D. D. Dietrich, F. Sannino, and K. Tuominen, Phys. Rev. D **72**, 055001 (2005).

[17] R. Foadi, M. T. Frandsen, and F. Sannino, arXiv:hep-ph/1211.1083.

[18] K. Lane and S. Mrenna, Phys. Rev. D **67**, 115011 (2003).

[19] T. Sjöstrand, S. Mrenna, and P. Z. Skands, JHEP **05**, 026 (2006).

[20] M. J. Oreglia, Ph.D. Thesis, SLAC-R-236 (1980), Appendix D., SLAC.

[21] J. E. Gaiser, Ph.D. Thesis, SLAC-R-255 (1982), Appendix F., SLAC.

[22] T. Skwarnickia, Ph.D. Thesis, F31-86-02 (1986), Appendix E., DESY.

[23] G. Cowan, K. Cranmer, E. Gross, and O. Vitells, Eur. Phys. J. C **71**, 1554 (2011).

[24] ATLAS Collaboration, (2012) arXiv:1209.2535.

[25] CMS Collaboration, (2012) arXiv:1206.0433.

[26] V. Abazov *et al.*, D0 Collaboration, Phys. Lett. B **671**, 349 (2009).

[27] K. D. Lane, Phys. Rev. D **60**, 075007 (1999).

[28] E. Eichten and K. Lane, Phys. Lett. B **669**, 235 (2008).